

Electron Cryomicroscopy and Computer Image Processing Techniques

Use in Structure–Function Studies of Rotavirus

B. V. Venkataram Prasad and Mary K. Estes

1. Introduction

Rotavirus (RV), a double-stranded (ds)RNA virus in the family Reoviridae, is a complex, relatively large (diameter, including spikes = 1000 Å), nonenveloped icosahedral virus. Once RV was recognized as a major human pathogen, it was extensively studied using modern molecular genetic and biological techniques, as discussed elsewhere in this book. These studies provided basic information about gene-coding assignments, protein processing, genome expression and replication, viral morphogenesis, and pathogenesis (*1*). In addition, molecular epidemiological studies, coupled with the characterization of neutralizing monoclonal antibodies (MAbs) and sequencing of the genes that encode the neutralizing antigens, provided an understanding at the molecular level of the antigenic and genetic variability of the RVs.

Medical relevance, intriguing structural complexity, and several unique strategies in the morphogenesis of RVs have provoked extensive structural studies on these viruses in recent years (*2–10*). A detailed architectural description of these complex viruses, including the topographical locations of the various structural proteins and their stoichiometric proportions, was obtained as the resolution of these techniques improved. Together with molecular biological studies, structural studies are permitting a dissection of the molecular mechanisms that underlie biological processes of the virus, such as cell entry, neutralization, transcription, gene expression, and virus assembly (*8*). This chapter reviews current knowledge of RV structure and the methods used in structural analysis.

From: *Methods in Molecular Medicine*, Vol. 34: *Rotaviruses: Methods and Protocols*
Edited by: J. Gray and U. Desselberger © Humana Press Inc., Totowa, NJ

2. Computer Image Processing of Electron Cryomicrographs

Over the past four decades, X-ray crystallography has been the technique of choice to study three-dimensional (3-D) structures of biological macromolecules and macromolecular assemblies at atomic resolution. Structures of several animal viruses have been studied using this technique (*11–12*; see *ref. 13* for a brief review of the technique). Until now, the largest structure that has been studied using this technique is simian vacuolating virus 40, ~500 Å in diameter (*14*). However, recently, the structure of bluetongue virus (BTV) cores, ~680 Å in diameter, a virus in another genus of the Reoviridae family, has been determined to near-atomic resolution, using X-ray crystallographic techniques (*15*). X-ray crystallographic techniques have also been used on individual viral proteins (VPs), such as the hemagglutinin and neuraminidase proteins of influenza virus (*12*), several proteins of HIV (*16,17*) and, most recently, VP6 of RV (*18*). Attempts are being made to determine the atomic resolution structure of the entire RV and subassemblies of RV using X-ray crystallographic techniques.

Prerequisite to successful structural analysis by X-ray crystallography is the ability to obtain crystals, of the specimen of interest, which diffract X-rays to atomic resolution. In the past decade, advances in electron cryomicroscopy (cryo-EM) and computer image processing techniques have provided another powerful tool for studying the 3-D structures of biological macromolecules and assemblies. This technique does not require the specimen to be in a crystalline state. Another advantage of this technique that it allows structural studies of the specimen not only in its native state, but also under various physiological conditions. For example, this technique has been used to study complexes of antibody-bound virus (*3,19–22*) and receptor-bound virus (*23*), transcribing virus (*9*), and specimens under varied chemical states, such as different pH and ionic strengths (*24*). All information obtained on structure–function relationships in RVs has come from using cryo-EM and computer image processing techniques. The following sections briefly discuss these techniques, and then describe how they have been useful in dissecting structure–function correlations in RVs.

2.1. Computer Image Processing

Because of the large depth of focus of conventional electron microscopes, transmission electron micrographs, in effect, represent two-dimensional (2-D) projections of the specimen. Inference of the detailed 3-D structure by direct examination of electron micrographs is therefore often a difficult task. Over the past two decades, computerized procedures have been developed to reconstruct the 3-D structure of a specimen from such projections. These procedures offer an objective way of extracting 3-D structural information from electron

micrographs. Similar procedures of reconstruction from projections are used in other contexts, such as diagnostic tomography.

To determine the 3-D structure of any object, it is necessary to combine the information content from different views of that object. These different views are sometimes provided by the specimen lying in different orientations, as in the case of icosahedral viruses, or they may be obtained by tilting the specimen in the microscope. 3-D reconstruction from electron micrographs is based on what is known as the projection theorem, which states that the 2-D Fourier transform of a projection of a 3-D object is a central section, normal to the direction of the view, of the 3-D Fourier transform of the object. If all the different orientations of the specimen can be identified with respect to a common frame of reference, the 3-D Fourier transform of the specimen can be built from the 2-D Fourier transforms of different views. Fourier inversion of the 3-D transform thus obtained gives the 3-D structure of the specimen.

For icosahedral viruses, Crowther et al. (25–27) have developed image-processing procedures to determine their 3-D structure from micrographs. The first step in the computer processing of electron micrographs is converting the image into digitized data by microdensitometry. Regions in the micrographs with a sufficient number of particles are digitized using a computer-controlled microdensitometer. The digitized regions are put into the computer, where each particle is windowed and centered inside a box. The orientation of each particle is determined in a computer from its Fourier transform using the so-called common lines procedure (26). Orientations of enough particles are determined so that they evenly represent the asymmetric unit of an icosahedron. The number of particles required for a reconstruction depends on the size of the specimen and the resolution sought. Typically, to attain a resolution of 20 Å for RV, 200 particles with unique orientations are used. For resolution closer to 10 Å, the number of particles with unique orientations have to be in the thousands. Particle images with well-determined orientation parameters are then combined in Fourier space using cylindrical expansion methods, to obtain a 3-D Fourier transform (26). An inverse Fourier transform then gives the 3-D structure. Orientation parameters of the particles are refined, either with respect to one another, using the cross-common lines, or with respect to the projections obtained from the initial 3-D map, in an iterative fashion. The visualization and interpretation of the 3-D reconstruction are carried out using computer graphics software. These procedures have been modified and refined in the past few years by several laboratories (27–31). A simplified outline of the image processing scheme is shown in **Fig. 1**. A detailed description of every aspect of the processing protocol is beyond the scope of this chapter but can be found in **ref. 29**. Computations of difference maps between closely related

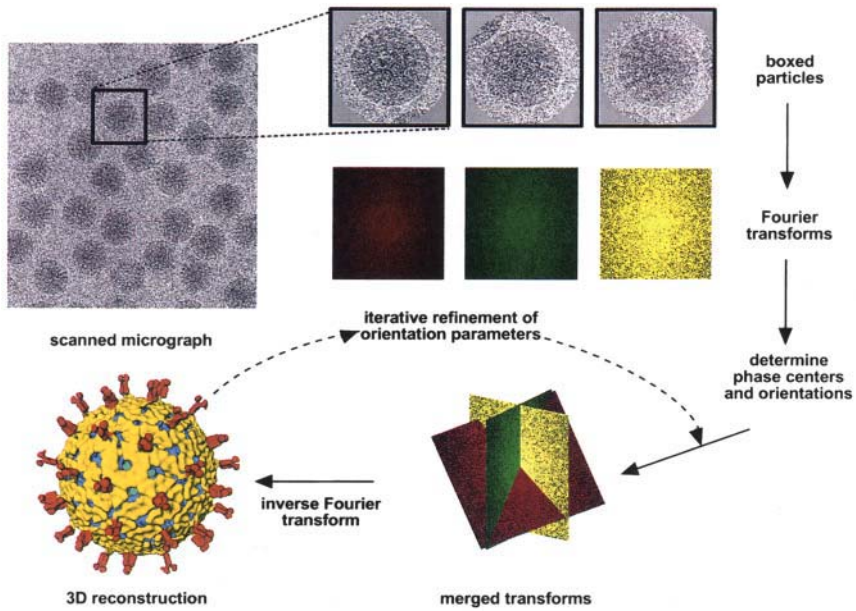


Fig. 1. A brief schematic representation of the major steps involved in the 3-D reconstruction of the RV structure.

strains (e.g., wild-type and mutant [4]), or viruses in different states (6), allow additional structural information to be obtained.

2.2. Electron Cryomicroscopy

In conventional transmission EM one normally uses metal-shadowing or negative-staining techniques to enhance image contrast. These preparative techniques may potentially alter the structure of the specimen, and sometimes may destroy fragile structural features because of chemical modification, dehydration, and desiccation. As a result, these preparative techniques are not suitable, particularly when the goal is to obtain 3-D structural information. However, for diagnostic purposes, these conventional techniques are adequate, and have proven very useful. In 1975, Taylor and Glaeser (32) introduced a method of embedding the specimen in a thin layer of ice, and imaging at low temperatures using a low electron dose. Since then, several laboratories have been involved in the improvement of this technique (for review, *see* ref. 33). Cryo-preparative techniques not only provide good contrast but also preserve the structural integrity of the specimen. One further advantage of structural analysis using electron images of ice-embedded specimens is the ability to retrieve the details of the internal structure of particles. This contrasts with

structure determination from images of negatively stained specimens, in which it is possible to obtain only surface features. The image contrast in the absence of stains or metal decoration is caused by the scattering density difference between protein and ice.

Cryo-EM involves three principal steps: quick-freezing of the specimen, transfer of the specimen to the microscope, and examination of the specimen in the microscope at low temperature. The first step is carried out using a mechanical guillotine-type plunging device (34). The specimen grid is held by a tweezer in the quick-freezing device. After the excess liquid on the grid is blotted using filter paper, the specimen grid is rapidly plunged into liquid ethane (cryogen) at its melting point. This rapid freezing produces a thin layer of vitreous or amorphous ice in which the specimen is embedded. In the second step, the frozen specimen is initially transferred to a cryospecimen holder maintained at liquid nitrogen temperature (-173°C) in a workstation. Then the cryo-specimen holder is quickly transferred to the electron microscope. The specimen is examined in the microscope at a temperature below -160°C , using low electron doses (typically $5\text{--}10\text{ e}^{-}/\text{\AA}^2$ on the specimen). Several technical problems associated with this technique have been addressed during the past few years, which have made this a successful technique (for details, *see* refs. 33,35).

2.3. Recent Developments in Cryo-EM

In recent years, there have been exciting developments in the high-resolution electron imaging of biological specimens: for example, the use of computer-controlled spot-scan imaging with medium-high-voltage electrons to reduce beam-induced motion images and to increase the efficiency of recording high resolution (7,36–39); the use of a field emission gun with intermediate-high-voltage electrons to increase the high-resolution image contrast by improving temporal and spatial coherence (40–42), and the use of energy-filtered electrons to remove the background intensity caused by inelastic scattering, and to increase the scattering signal from the specimen (43). Advances in computer image processing schemes have also been made, taking advantage of high-speed, high-performance computers and multiprocessor computers (44). The future looks promising for attaining 10 \AA resolution and higher by cryo-EM, for icosahedral particles. The structure of the hepatitis B virus has already been determined to a resolution of $\sim 8\text{ \AA}$, using cryo-EM techniques (41,42).

2.4. Combined Use of X-ray Crystallography and Cryo-EM Techniques

An exciting trend in recent years is the marriage of X-ray crystallography and cryo-EM techniques (45). Several studies have shown that these two

techniques are not mutually exclusive, but can effectively complement one another, particularly in studying large macromolecular assemblies. If the structures of individual components of an assembly are available at atomic resolution, this information can be fitted into the structure of the whole assembly determined by cryo-EM techniques, to enhance understanding of the molecular interactions. The complementarity of these two techniques offers a significant step forward in structural biology, as is shown in structural studies on such viruses as adenovirus (46), flock-house virus (47), rhinovirus (48), and Sindbis virus (49). Recent structural analysis of the BTV core is an excellent example of the combined use of cryo-EM and X-ray crystallography techniques to determine the structure of a complex macromolecular assembly at atomic resolution (50). Similarly, the cryo-EM structure of Norwalk virus has been very useful for determining the structure at atomic resolution of this virus by X-ray crystallographic data (51). Such a combinatorial approach is being used not only on icosahedral viruses, but also in the structural studies of ribosomes (52), which lack any symmetry, and other nonicosahedral complex structures, such as bacteriophage $\phi 29$ (53).

3. 3-D Structure of RV

3-D structural studies using cryo-EM techniques have been carried out on two RV strains: simian RV SA11 (2–4) and rhesus RV (5,6). The structural features seen in these two strains of RV are very similar, because both have three concentric layers of protein. A surface representation of a 3-D reconstruction of triple-layered (mature) RV along the icosahedral threefold axes is shown in **Fig. 2A**. Some of the structural features inside the RV structure are shown in a cross-sectional slice taken from the 3-D reconstruction of RV in **Fig. 2B**.

The structure, which is based on a left-handed $T = 13$ icosahedral lattice, exhibits distinct structural features, including aqueous channels and surface spikes. The overall diameter of the particle, including the spikes, is 1000 Å.

3.1. Outer Layer

Biochemical experiments have shown that the outer shell of the RV contains two proteins, VP7 and VP4 (54,55). The major component is VP7, a glycoprotein. A close examination of surface features (**Fig. 2A**) indicates that VP7 molecules cluster into triangular-shaped trimers surrounding the aqueous channels, on the $T = 13$ icosahedral lattice. The VP7 trimers have a small depression at the center, and they are connected to one another on the sides. Whether VP7 molecules aggregate into trimers prior to the assembly of the shell is not known, nor whether they cluster into trimers on their assembly into the icosahedral shell. The $T = 13$ icosahedral symmetry of the VP7 layer dictates that each virion has 780 molecules (or 260 trimers) of VP7. The overall thickness of the VP7 layer is ~ 35 Å.

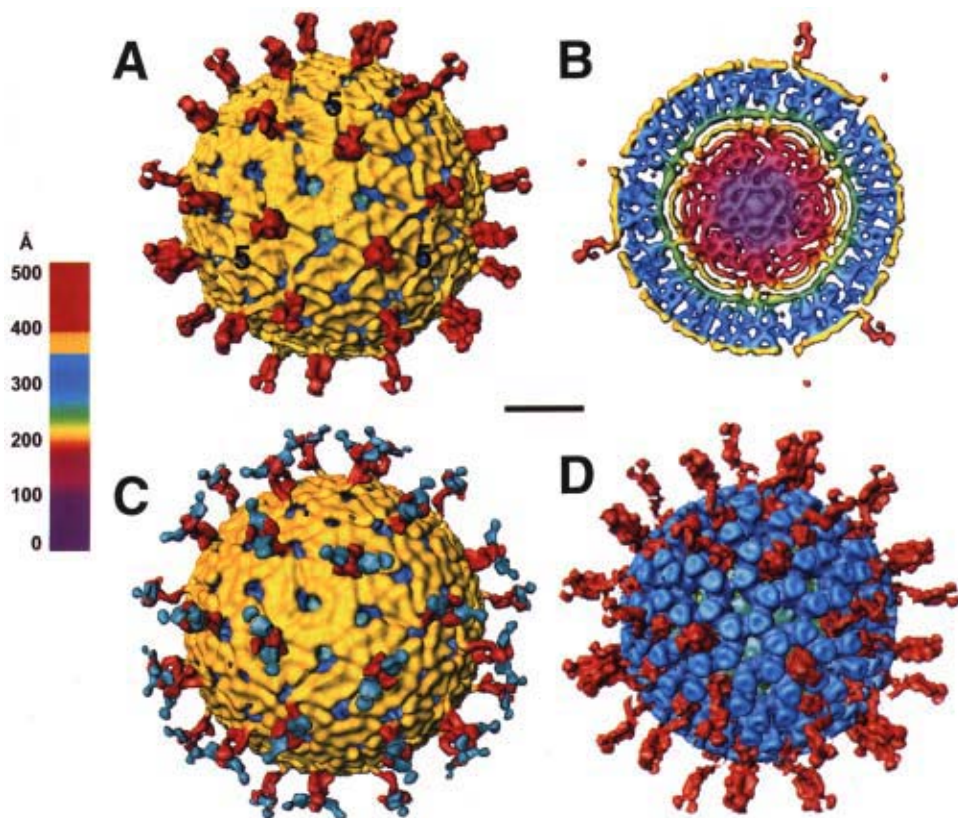


Fig. 2. (A) 3-D structure of the triple-layered particle (TLP) at a resolution of 23 Å. A set of icosahedral symmetry axes and the locations of the three types of channels are indicated. The surface is a left-handed $T = 13$ icosahedral lattice. In such a lattice, a fivefold axis is reached from its neighboring fivefold axis by stepping over three six-coordinated positions and taking a left turn. (B) Central cross section extracted from the 3-D map of the virus. The mass density breaks up into three distinct shells between the radii of 210 and 500 Å. These three shells are between the radii 500 and 340 Å, 340 and 270 Å, and 270 and 210 Å. The VP4 spike density is also shown; notice the lower domain of VP4 inside one of the channels. (C) Surface representation of the 3-D structure with anti(VP4) Fab bound. (D) Interaction of VP4 spikes with the VP6 layer. Scale bar = 20 Å.

3.2. Aqueous Channels

A distinctive feature of the RV structure is the presence of aqueous channels at all of the five- and six-coordinated positions on the $T = 13$ icosahedral lattice (see Fig. 2A). These channels penetrate into the outer two layers of the structure and are ~140 Å deep. They have been classified into three types based on their location with respect to the icosahedral symmetry axes. Type I channels run down the icosahedral fivefold axes, type II channels are those on the

six-coordinated positions surrounding the fivefold axes, and type III channels are those on the six-coordinated positions neighboring the icosahedral threefold axes. In each virion, there are 132 channels: 12 type I, 60 type II, and 60 type III channels. Type II and III channels are about 55-Å wide at the outer surface of the virus. The type I channels, in contrast, have a narrower and more circular opening of ~40 Å in diameter. All the channels constrict before widening in the interior, and have their maximum width at the position close to the surface of the inner shell proteins, as seen in the side view of the type III channels in **Fig. 2B**.

3.3. Surface Spikes

Another distinctive feature of the RV structure is surface spikes. From the surface of the particles, 60 spikes extend to a length of 120 Å (**Fig. 2A**). The RV spikes are located at the outer edge of the type II channels that surround the icosahedral fivefold axes. Each spike has a distinct bilobed structure at the distal end. Each lobe has a diameter of ~25 Å. These lobes are individually connected to rod-shaped densities that are separated from each other by a hole that is ~20 Å in diameter. These rod-shaped densities, with a left-handed helical twist, merge together as they approach the surface of the outer layer, making two points of contact with the vertices of the triangular-shaped VP7 trimers.

When the spikes on RV were first discovered, Prasad et al. (2) predicted that these surface projections were made up of VP4, which was confirmed by immunolabeling studies using MAbs against VP4 (3). Two antigen-binding fragments (Fab) molecules bound to the sides of the distal bilobes of each spike (**Fig. 2C**). The volume of the spike indicates that each spike can accommodate two molecules of VP4. Thus, each virion contains 120 copies of VP4. The observed structural features of individual spikes, as described above, and in vivo radiolabeling studies, further support the idea that the spikes are dimers of VP4 (4). Gel filtration analyses of expressed VP4 also have provided biochemical evidence that VP4 is an oligomer, probably a dimer. Interactions between these oligomers are apparently maintained by hydrophobic interactions, because these are readily disrupted by detergents (56), which explains why dimers of VP4 have not been detected by simple analysis of VP4 in virus disrupted by sodium dodecylsulfate (SDS) and separated by SDS-polyacrylamide gel electrophoresis.

3.4. Internal Domain of VP4

From the 3-D structure of the native virus alone, it is not possible to determine whether there is an inward extension of the VP4 spikes. That is, do the spikes terminate at the surface of the virion, or do they penetrate into the VP7 layer? Based on the volume of VP4 calculated from the 3-D reconstructions of

the native and the Fab-bound virions, Prasad et al. (3) estimated that about 30 kDa of VP4 is buried inside the virion surface. By computing a difference map between the structures of the native strain and a reassortant strain of RV that lacks spikes, the existence of a large internal domain of VP4 beneath the VP7 surface was confirmed (4). This domain of VP4 is centered inside the type II channel, in close association with the walls of the channel made of trimers of VP6, as shown in **Fig. 2D** (the structure of the VP6 shell is described in more detail in **Subheading 3.5.**). Similar results were obtained by difference imaging of the virus structure at normal pH and alkaline pH (6). At alkaline pH, the RV spikes fall off without affecting the integrity of the VP7 layer (6,57). The finding that VP4 interacts extensively with the VP6 layer may have implications in the morphogenesis of the RV particles. Shaw et al. (4) have suggested that VP4 may play an important role, along with the nonstructural protein (NSP4), in facilitating the budding of progeny double-layered particles (DLPs) through the endoplasmic reticulum (ER) membrane, and that assembly of VP4 onto newly made particles occurs prior to VP7 assembly.

An interesting aspect of RV infection is trypsin-enhanced infectivity (54,58). Trypsin, present at the natural site of infection, cleaves VP4 at a conserved arginine residue to produce VP8* (28 kDa, aa 1–247) and VP5* (~60 kDa, aa 248–776). Trypsin cleavage of VP4 is accompanied by a significant increase in RV infectivity (54,58), which is associated with enhanced cell entry (59,60). Although the overall structure of the VP4 spike is visualized in the cryo-EM reconstructions, the topographical locations of the proteolytic fragments VP5* and VP8* are not known. The MAb that was used in the structural studies by Prasad et al. (3), 2G4, is a VP5*-specific antibody, which binds to the sides of the distal lobes of the VP4-spike, suggesting that these distal globular domains of VP4 contain some portions of VP5*. The MAb 2G4 is a neutralizing antibody, and has been shown to block virus penetration, but not cell attachment. The exposed region of the distal tip of the spike is probably involved in initial attachment to cells, and the region of the spike binding to 2G4 molecules may be involved in cell penetration.

3.5. The Intermediate Layer

Treatment of intact triple-layered virions with chelating agents (e.g., ethylenediamine tetra-acetic acid) removes the outer shell, reduces infectivity by several log steps, and exposes the inner shell proteins. The resulting DLPs are indistinguishable from those produced in infected cells (61). Electron micrographs of DLPs embedded in vitreous ice show that these particles are 705 Å in diameter, with a bristly surface. The 3-D structure of the DLPs (**Fig. 3A**) has been determined to ~19 Å, using cryo-EM techniques (7). The protein mass is mostly concentrated into 260 morphological units positioned at

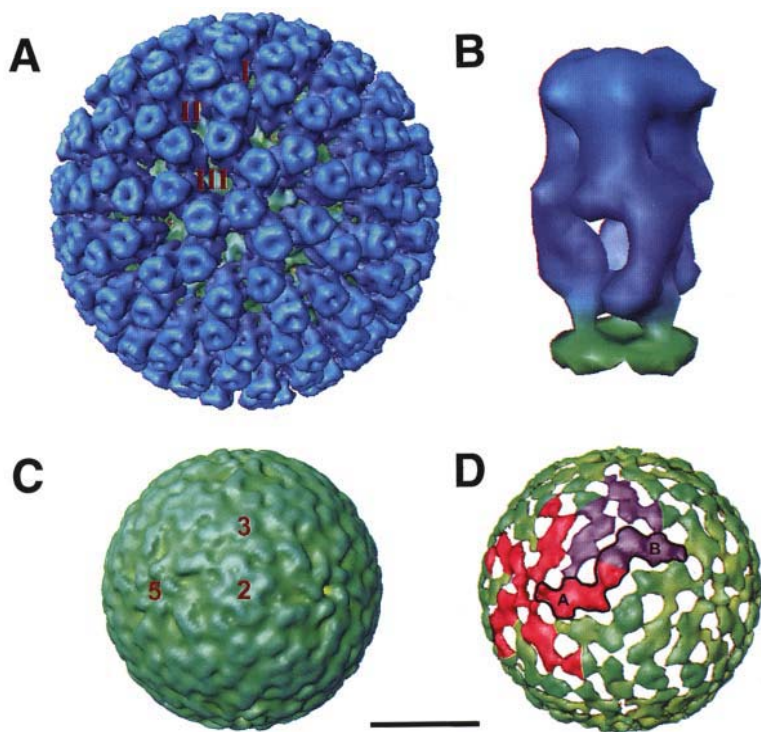


Fig. 3. (A) Surface representation of the 3-D structure of the double-layered particle (DLP) at a resolution of ~ 19 Å. A set of icosahedral symmetry axes and the locations of the three types of channels are indicated. (B) VP6 computationally isolated from the 3-D map of the DLP. (C) Surface representation of the VP2 layer extracted from the structure of DLP; the threshold used represents 120 molecules of VP2. (D) As viewed at a higher threshold, the boundaries of two molecules of VP2 that make the icosahedral asymmetric unit are denoted as A and B. Scale bar = 200 Å.

all the local and strict threefold axes of the $T = 13$ icosahedral lattice. The location and shape of the capsomeres strongly suggest a trimeric clustering of the inner capsid protein, VP6. This has been confirmed by separating VPs on nondenaturing conditions (62,63). These 260 capsomeric units are arranged in such a way that there are channels at all five- and six-coordinated centers. These channels are in register with the channels in the VP7 layer. The structure of the VP6 molecule (Fig. 3B) appears to have two domains: the globular upper domain, and a slender lower domain.

The upper globular domains of individual monomers interact with one another in stabilizing the trimer. The sides of the lower domain seem to be involved in intercapsomeric interactions, and the bottom part of the lower domain interacts

with the VP2 layer. VP6 molecules interact with VP7 through their upper domain. Flat upper domains of the VP6 trimers protrude into the VP7 layer, so that the close contact between the two shells occurs primarily around the local and strict threefold axes. The triangular-shaped VP7 trimers spread across the VP6 trimers, and portions of the VP6 trimers are visible through the outer-shell channels (**Fig. 2A**). It is possible that small molecules or small enzymes may be able to interact with portions of the VP6 layer, even in the presence of the outer VP7 layer. Consistent with this idea, at least one MAb to VP6 has been shown to bind to both triple-layered particles and DLPs (**64**).

Recently, the structure of VP6 has been determined by X-ray crystallographic analysis to 2.8 Å (**18**). The tertiary structure of VP6 bears several similarities to the structure of VP7 of BTV (**65**), which is the counterpart of VP6 in RV. Both these proteins consist of two distinct domains: a distal eight-stranded β -barrel domain and a lower α -helical domain. The distal β -barrel domain interacts with VP7; the α -helical domain interacts with VP2. Fitting of the X-ray structure of VP6 into the cryo-EM structure of RV is in progress, to delineate the regions of VP6 that interact with VP7, VP4, and VP2.

3.6. Inner Layer

Although early protein and EM analyses defined the composition of the outer two layers of the virion with certainty, the existence and composition of the third shell initially was based on conjecture. The total mass density in the outer shell accounts for 780 and 120 molecules of VP7 and VP4, respectively. The volume of the protein in the intermediate shell accounts for 780 molecules of VP6. On the basis of the radial density profile, and the fact that VP2 is the most abundant of the remaining three structural proteins, it was proposed that the density between the radii of 230 and 270 Å is caused by the shell formed by VP2 molecules (**66**). The existence of an inner shell was confirmed when single-layered (core-like) particles were produced by expression of VP2 alone (**67**).

3-D structural analysis of recombinant particles containing VP2 alone (2-virus-like particles [VLPs]) has indicated that the VP2 layer extends from a radius of about 230 Å to 270 Å, in agreement with interpretation based on the radial density profile computed from the 3-D structure of the virion. The structure determination of 2-VLPs to a resolution closer to ~20 Å has been hampered by extensive aggregation of 2-VLPs. However, knowing the radial extension of the VP2 layer, the structural features of the VP2 layer has been deduced from the reconstruction of native RV particles or recombinant particles (**68**) containing VP2 and VP6, referred to as 2/6-VLPs (**10**). In contrast to the VP7 and VP6 layers, the VP2 layer is a rather featureless, continuous bed of density (**Fig. 3C**). Examination of the structure of this layer at a slightly higher

threshold of protein mass reveals the arrangement of 120 VP2 molecules on the $T = 1$ icosahedral lattice (**Fig. 3D**). Each asymmetric unit of the icosahedron consists of two molecules, referred to as type A and type B monomers. The type A monomer lies close to the fivefold axis, the type B monomer originates slightly away from the fivefold axis, and extends toward the threefold axis. The $T = 1$ icosahedral organization, with 120 molecules, poses an interesting structural question about how this layer, consisting of 120 molecules, interacts with the VP6 layer, consisting of 780 molecules. Such a $T = 1$ icosahedral structure, with 120 molecules, is unique, because it renders the two molecules in the asymmetric unit quasiequivalent, and has been observed in other dsRNA viruses besides RV. In the Reoviridae family, both aquareovirus (**69**) and BTV (**15**) have inner layers composed of 120 subunits on a $T = 1$ icosahedral lattice. A $T = 1$ symmetry with dimers is also observed in other dsRNA viruses outside Reoviridae: The fungal viruses L-A of *Saccharomyces cerevisiae* and P4 of *Ustilago maydis* exhibit similar organization (**70**). This unique $T = 1$ organization may be of fundamental significance in the endogenous transcription of the genome of dsRNA viruses.

3.7. Internal Organization

In addition to VP7, VP4, VP6, and VP2 reviewed so far, the RV structure should account for VP1 and VP3, the remaining structural proteins, and the genomic RNA. In the 3-D structure of RV, several internal features are seen. To understand the internal organization of RV and to interpret the internal structural features in terms of minor proteins and the genomic RNA, a twofold strategy was used by Prasad et al. (**7**). First, difference imaging between native DLPs and various recombinant VLPs was used to identify the internal features. Second, a higher-resolution (~ 19 Å) structure of the DLP was carried out, to delineate the internal features more clearly.

3.7.1. Locations of VP1 and VP3

Although VP1 and VP3 are present in small amounts, they play an important role in the endogenous transcription process of RV. Several biochemical studies have indicated that VP1 is the RNA-dependent RNA polymerase (**71**) and VP3 is the guanylyltransferase (**72**). The structure of 1/2/3/6-VLPs shows flower-shaped features attached to the inside tip of the VP2 at all the fivefold positions (**Fig. 4B**), which is absent in 2/6-VLPs (**Fig. 4A**); it is also absent in 1/2/6-VLPs and 3/2/6-VLPs. These studies suggest that the flower-shaped feature becomes discernible only when VP1 and VP3 are both present, and that this structural feature represents a complex of VP1 and VP3. Although these studies strongly suggest the location of VP1 and VP3, the observed shape of the proposed VP1–VP3 is uncertain, because of the reconstruction procedures that

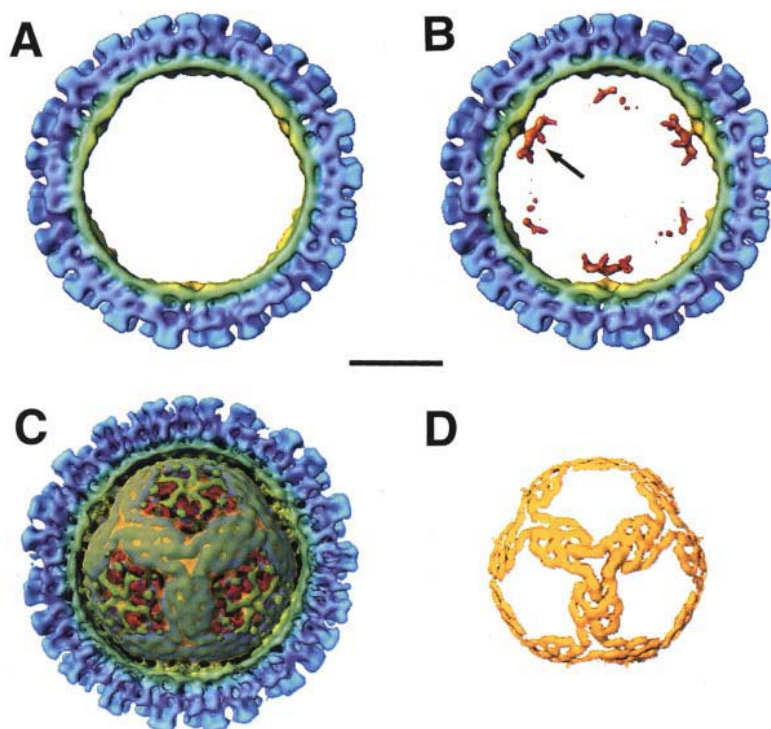


Fig. 4. **(A)** Identical cross-section of 2/6-VLP structure. Notice the absence of the flower-shaped structural feature seen in B. **(B)** Cross-section (85 Å thick) of 1/2/3/6-VLP structure. Flower-shaped structures are seen attached to the inside surface of VP2 at all the icosahedral fivefold axes. **(C)** Cutaway from the 19-Å structure of the DLP, exposing the mass density caused by the genomic RNA. **(D)** Dodecahedral shell of the ordered RNA, extracted from the 19-Å structure. Scale bar = 200 Å.

implicitly use icosahedral symmetry. The shape that has been observed can only be real if each virion has 60 molecules of VP1–VP3, or this flower-shaped complex has an internal fivefold symmetry. The volume occupied by each flower-shaped structure, assuming a protein density of 1.30 g/cm³, accounts for about 25% of the expected mass of a complex of VP1 (125 kDa) and VP3 (98 kDa). Biochemical data indicate that there are 12 molecules of VP1 and 12 VP3 molecules per virion (72). The remaining portions of VP1 and VP3 may extend further inside the radius of 160 Å, and are transparent to structural analysis, either because they are disordered or because they move away from the fivefold axes, and lack any semblance of icosahedral symmetry. Thus, the flower-shaped structure may represent the structurally discernible portion of the VP1–VP3 enzyme complex.

3.7.2. Location of Genomic RNA

Comparison of the radial density profiles computed from the structures of DLPs and VLPs clearly indicate that mass density caused by the genomic RNA lies inside the radius of 230 Å (7). At this radius, the DLP structure shows strong mass density surrounding the fivefold axes, and between the neighboring threefold axes (**Fig. 4C**). This mass density is completely absent in the 2/6-VLP and the 1/3/2/6-VLP structures. The density attributed to ordered RNA in the 23-Å DLP is clearly resolved into parallel strands of tube-like mass density that form a dodecahedral shell in the 19 Å structure of the DLPs, determined using micrographs taken by using a 400 keV electron microscope. These tubes of mass density have an average diameter of 20 Å, typical of a dsRNA double helix (**Fig. 4D**). These strands encircle the VP1–VP3 complex located at the fivefold axis. Icosahedral packing of RNA does not imply 60-fold repetition in the gene sequence, but indicates that portions of the dsRNA occupy an icosahedrally equivalent volume in the structure. Icosahedrally ordered nucleic acid has been previously observed in small virus structures by X-ray crystallography (73–77). The maximum number of base pairs previously visualized in a virus structure is about 300 (76). In the RV structure, ordered RNA accounts for ~4500 of a total 18,555 bp.

The 19 Å-DLP structure shows that there are several points of contact between the inwardly protruding portions of VP2 and the RNA surrounding each fivefold axis (7). These observations are consistent with biochemical results that show VP2 has dsRNA binding activity (78). Thus, VP2, which is icosahedrally assembled,

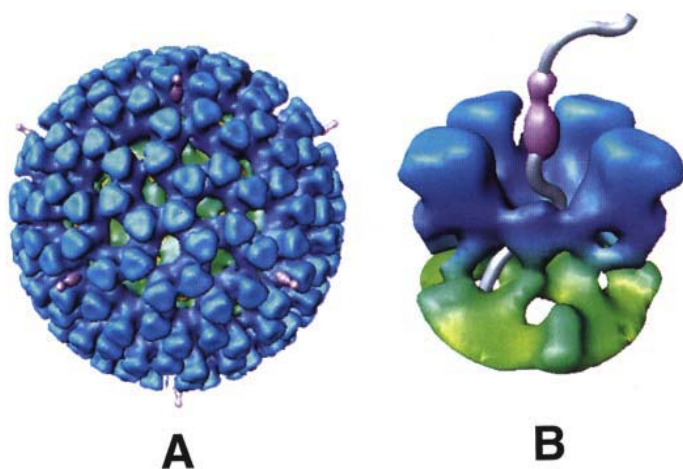


Fig. 5. (A) 3-D structure of transcribing DLP. (B) Proposed pathway for the nascent mRNA molecule exiting through a type I channel.

appears to be responsible for inducing icosahedral ordering on closely interacting portions of RNA. Such extensive ordering of dsRNA is also seen in the recently determined X-ray structure of the BTV core (15), which is the equivalent of the RV DLP.

The extensive ordering of the genome, described above, is perhaps critical for endogenous transcriptase activity. It may facilitate an orchestrated movement of the genome through the enzyme complex. This motion could be driven by the continuous exit of newly synthesized mRNA. The pores surrounding the fivefold axes, in the VP2 layer, are large enough to permit mRNA to exit, although it is also possible that VP2 may undergo conformational changes during transcription, to facilitate the exit of mRNA. Understanding of this process will be made clear by observing changes in the RNA and the VPs during active transcription, and also under conditions in which the DLP has been rendered transcriptionally incompetent. Though it has not been possible, from any of the current structural studies, to address the question of where the different segments of dsRNA are located inside the structure, it is tempting to speculate that a substantial portion of each of the 11 segments is ordered around a fivefold axis, and that each segment interacts with a specific VP1–VP3 complex.

3.8. Structure of Actively Transcribing DLPs

From earlier studies, the authors had postulated that channels in the capsid layers would be used for the import of the precursors necessary for transcription and the exit of nascent mRNA molecules (2). As described in **Subheading 3.5.**, there are 132 channels in the VP6 layer. Which of these channels are used for export of the nascent transcripts? To determine how the mRNA transcripts are translocated through the intact DLPs during transcription, the 3-D structure of actively transcribing DLPs has been determined (9). There are two chief inferences from these studies: First, the DLPs remain structurally intact during transcription; second, the nascent transcripts exit through the type I channels in the VP6 layer (**Fig. 5A**). The observation that the DLPs remain structurally intact is especially important, considering that the particles are capable of unlimited transcription, provided that the necessary RNA precursors are continuously supplied (79). The structural integrity of the particles is suggested not only from the images and the reconstruction, but also from the observation that the comparison of particle images with projections of the reconstruction by cross-common lines yields phase residual values that are very similar to those observed for nontranscribing DLPs. These results strongly imply that icosahedral symmetry is maintained to the same degree in both structures, at least to the resolution that these structures have been analyzed.

Why is the structural integrity of DLP necessary for transcription? Biochemical studies show that no structural protein by itself is capable of carrying

out transcription, which occurs within the confines of the intact DLPs. Structural and biochemical studies seem to indicate that the VP2 protein may play a scaffolding role in the architecture of RV. The inner surface of the VP2 layer not only provides a structural support for the RNA, but also helps to properly position the transcription complex consisting of VP1 and VP3. Recent biochemical studies have shown that the amino terminus of the VP2 molecule possesses nonspecific single-stranded RNA and dsRNA binding activity, and also that it is essential for the incorporation of VP1 and VP3 (80). Structural analysis of 2/6-VLPs, with an intact and a truncated amino-terminus of VP2, have shown that the amino-terminus is located at the inside surface of the VP2 layer, and close to the fivefold axis (10). The unique arrangement of VP2 molecules on a $T = 1$ icosahedral lattice, discussed previously (Fig. 3D), may be particularly useful in carrying out the dual roles of providing structural support to the RNA and transcription complex. It is likely that type A monomers of VP2, as they interact in a head-to-head manner at the fivefold axis, are exclusively involved in the interactions with VP1 and VP3, which are anchored to the inner surface of the VP2 capsid layer, along the fivefold axis; the N-terminal portions of type B monomers may provide the necessary interactions with RNA.

The outer surface of the VP2 layer provides a structural platform for the assembly of VP6 trimers, preventing aggregation of the core particles (VP2, VP1, VP3, and the genome), which are known to be highly hydrophobic (81). The assembly of VP6 provides well-defined conduits for the exiting RNA molecules. From structural and biochemical studies, it can be hypothesized that the structural integrity of the DLP is necessary for the observed transcriptional efficiency and continuous reinitiation, because of the need to hold the components of the transcription machinery in their proper arrangements throughout repeated cycles of initiation–elongation, as well as to enable the efficient and continuous release of the mRNA transcripts.

3.9. Model for Exit Pathway of mRNA

Although structural studies on the actively transcribing particle strongly suggest that the type I channels are used for exporting the nascent mRNA molecules, the precise pathway from the site of synthesis to the exterior of the particle remains to be elucidated. Based on the observed internal organization (7), and the structure of the transcribing particle, a model for the exit pathway in RV has been proposed (9). The RNA synthesis probably occurs within the core of the virion, very near to the fivefold axes, because this is the location of the transcriptional complexes composed of VP1 and VP3. Newly transcribed mRNA then exits the core through the channels in the VP2 layer, which are immediately adjacent to the fivefold axis, and probably in clos-

est proximity to the site of synthesis. Once through the VP2 layer, the exiting strands of mRNA migrate out of the particle through the type I channels (at the fivefold axes) in the VP6 layer (**Fig. 5B**). In the electron images of the actively transcribing particles, 3–4 strands of mRNA, associated with the particles, have been observed (9). From these observations, it appears that multiple mRNA transcripts can be released simultaneously from an actively transcribing particle. Each genome segment may be transcribed by a specific polymerase complex, and the resulting transcript may exit the particle through the channel system at the fivefold axis adjacent to its site of synthesis. The mechanism of transcription and mRNA release proposed in these studies might also explain why no dsRNA virus with more than 12 genome segments has ever been found. 3-D structural studies using cryo-EM, similar to those described by Lawton et al. (9) on transcribing RV particles, have been carried out on orthoreoviruses (M. Yeager, personal communication). These studies have confirmed the finding of earlier studies using classical Kleinschmidt techniques, that the mRNA release occurs through the fivefold vertices in these viruses (82). In orthoreoviruses, the transcription complex is also suggested to be anchored to the inner surface of the innermost capsid layer at the fivefold axes (83). The release of mRNA through the fivefold vertices is probably a common characteristic of segmented dsRNA viruses, including BTV (15,84), aquareovirus (69), and the bacteriophage $\phi 6$ (85).

4. Conclusions and Future Challenges

Structural studies on RVs have helped to provide a foundation for understanding the molecular mechanisms underlying some of the functions of these viruses, and are just the beginning of obtaining a detailed understanding of the structure–function relationships in this complex and large virus. Present and future studies are aimed at answering several questions. Are there specific receptors for RVs and how do these viruses initiate the cell-entry process? How does the transcription take place inside intact DLPs? How does the virus encapsidate a correct set of genome segments? What are the roles of the nonstructural proteins in virus replication and self-assembly, and what molecular interactions regulate their functions? What is the molecular mechanism of budding of the progeny DLPs into the ER membrane?

The authors anticipate that a more complete picture of how these viruses replicate will emerge as structural analyses improve in resolution, either by cryo-EM or X-ray crystallography, or combinations thereof, in conjunction with advances in biochemical and molecular biological studies. Obtaining detailed molecular and structural information should also allow the development of more effective strategies to combat, prevent, or treat the clinical outcome of infections with these viruses. Increasing knowledge of the structure and

function of the RV genes and proteins, and the ability to produce VLPs of various components, are already being exploited to develop interesting vaccine candidates (*see* Chapters 3 and 9).

Acknowledgments

The authors' work is supported in part by grants from the NIH (AI 36040 and DK 31044), the W. M. Keck Foundation and the National Center for Research Resources (RR 02250). We thank J. Lawton and B. Pesavento for useful discussions and their help in making the figures.

References

1. Estes, M. K. (1996) Rotaviruses and their replication, in *Virology* (Fields, B. N., Knipe, D. M., and Howley, P. M., eds.), Lippencott Raven, Philadelphia, pp. 1625–1655.
2. Prasad, B. V. V., Wang, G. J., Clerx, J. P., and Chiu, W. (1988) Three-dimensional structure of rotavirus. *J. Mol. Biol.* **199**, 269–275.
3. Prasad, B. V. V., Burns, J. W., Marietta, E., Estes, M. K., and Chiu, W. (1990) Localization of VP4 neutralization sites in rotavirus by three-dimensional cryo-electron microscopy. *Nature* **343**, 476–479.
4. Shaw, A. L., Rothnagel, R., Chen, D., Ramig, R. F., Chiu, W., and Prasad, B. V. V. (1993) Three-dimensional visualization of the rotavirus hemagglutinin structure. *Cell* **74**, 693–701.
5. Yeager, M., Dryden, K. A., Olson, N. H., Greenberg, H. B., and Baker, T. S. (1990) Three-dimensional structure of rhesus rotavirus by cryoelectron microscopy and image reconstruction. *J. Cell Biol.* **110**, 2133–2144.
6. Yeager, M., Berriman, J. A., Baker, T. S., and Bellamy, A. R. (1994) Three-dimensional structure of the rotavirus haemagglutinin VP4 by cryo- electron microscopy and difference map analysis. *EMBO J.* **13**, 1011–1018.
7. Prasad, B. V. V., Rothnagel, R., Zeng, C. Q., Jakana, J., Lawton, J. A., Chiu, W., and Estes, M. K. (1996) Visualization of ordered genomic RNA and localization of transcriptional complexes in rotavirus. *Nature* **382**, 471–473.
8. Prasad, B. V. V. and Estes, M. K. (1997) Molecular basis of rotavirus replication: structure-function correlations, in *Structural Biology of Viruses* (Chiu, W., Burnett, R., and Garcia, R., eds.), Oxford University Press, New York and Oxford, pp. 239–268.
9. Lawton, J. A., Estes, M. K., and Prasad, B. V. V. (1997) Three-dimensional visualization of mRNA release from actively transcribing rotavirus particles *Nature Struct. Biol.* **4**, 118–121.
10. Lawton, J. A., Zeng, C. Q., Mukherjee, S. K., Cohen, J., Estes, M. K., and Prasad, B. V. V. (1997) Three-dimensional structural analysis of recombinant rotavirus-like particles with intact and amino-terminal-deleted VP2: implications for the architecture of the VP2 capsid layer. *J. Virol.* **71**, 7353–7360.
11. Rossmann, M. G. and Johnson, J. E. (1989) Icosahedral RNA virus structure. *Annu. Rev. Biochem.* **58**, 533–573.

12. Harrison, S., Skehel, J. J., and Wiley, D. (1996) Virus structure, in *Fields Virology* (Fields, B. N., Knipe, D. M. and Howley, P. M., eds.), Lippincott Raven, Philadelphia, pp. 59–99.
13. Baker, T. S. and Johnson, J. E. (1997) Principles of virus structure determination, in *Structural Biology of Viruses* (Chiu, W., Burnett, R., and Garcia, R., eds.), Oxford University Press, New York and Oxford, pp. 38–79.
14. Liddington, R. C., Yan, Y., Moulai, J., Sahli, R., Benjamin, T. L., and Harrison, S. C. (1991) Structure of simian virus 40 at 3.8-Å resolution. *Nature* **354**, 278–284.
15. Grimes, J. M., Burroughs, J. N., Gouet, P., Diprose, J. M., Malby, R., Zientara, S., Mertens, P. C. P., and Stuart, D. I. (1998) The atomic structure of the bluetongue virus core. *Nature* **395**, 470–478.
16. Hodge, C. N., Straatsma, T. P., McCammon, J. A., and Wlodawer, A. (1997) Rational design of HIV protease inhibitors, in *Structural Biology of Viruses* (Chiu, W., Burnett, R., and Garcia, R., ed.), Oxford University Press, New York and Oxford, pp. 451–473.
17. Kwong, P. D., Wyatt, R., Robinson, J., Sweet, R. W., Sodroski, J., and Hendrickson, W. A. (1998) Structure of an HIV gp120 envelope glycoprotein in complex with the CD4 receptor and a neutralizing human antibody. *Nature* **393**, 648–659.
18. Petitpas, I., Lepault, J., Vachette, P., Charpilienne, A., Mathieu, M., Kohli, E., Pothier, P., Cohen, J., and Rey, F. A. (1998) Crystallization an preliminary x-ray analysis of rotavirus protein VP6. *J. Virol.* **72**, 7615–7619.
19. Wang, G. J., Porta, C., Chen, Z. G., Baker, T. S., and Johnson, J. E. (1992) Identification of a Fab interaction footprint site on an icosahedral virus by cryoelectron microscopy and X-ray crystallography. *Nature* **355**, 275–278.
20. Smith, T. J., Olson, N. H., Cheng, R. H., Chase, E. S., and Baker, T. S. (1993) Structure of a human rhinovirus-bivalently bound antibody complex: implications for viral neutralization and antibody flexibility. *Proc. Natl. Acad. Sci. USA* **90**, 7015–7018.
21. Smith, T. J., Cheng, R. H., Olson, N. H., Peterson, P., Chase, E., Kuhn, R. J., and Baker, T. S. (1995) Putative receptor binding sites on alphaviruses as visualized by cryoelectron microscopy. *Proc. Natl. Acad. Sci. USA* **92**, 10,648–10,652.
22. Trus, B. L., Newcomb, W. W., Booy, F. P., Brown, J. C., and Steven, A. C. (1992) Distinct monoclonal antibodies separately label the hexons or the pentons of herpes simplex virus capsid. *Proc. Natl. Acad. Sci. USA* **89**, 11,508–11,512.
23. Olson, N. H., Kolatkar, P. R., Oliveira, M. A., Cheng, R. H., Greve, J. M., McClelland, A., Baker, T. S., and Rossmann, M. G. (1993) Structure of a human rhinovirus complexed with its receptor molecule. *Proc. Natl. Acad. Sci. USA* **90**, 507–511.
24. Wang, G. J., Hewlett, M., and Chiu, W. (1991) Structural variation of La Crosse virions under different chemical and physical conditions. *Virology* **184**, 455–459.
25. Crowther, R. A., DeRosier, D. J., and Klug, A. (1970) The reconstruction of a three-dimensional structure from projections and its applications to electron microscopy. *Proc. Roy. Soc. Lond. A* **317**, 319–340.

26. Crowther, R. A. (1971) Procedures for three-dimensional reconstruction of spherical viruses by Fourier synthesis from electron micrographs. *Philos. Trans. R. Soc. Lond. B. Biol. Sci.* **261**, 221–230.
27. Crowther, R. A., Henderson, R., and Smith, J. M. (1996) MRC image processing programs. *J. Struct. Biol.* **116**, 9–16.
28. Lawton, J. A. and Prasad, B. V. V. (1996) Automated software package for icosahedral virus reconstruction. *J. Struct. Biol.* **116**, 209–215.
29. Fuller, S. D., Butcher, S. J., Cheng, R. H., and Baker, T. S. (1996) Three-dimensional reconstruction of icosahedral particles—the uncommon line. *J. Struct. Biol.* **116**, 48–55.
30. Baker, T. S. and Cheng, R. H. (1996) A model-based approach for determining orientations of biological macromolecules imaged by cryoelectron microscopy. *J. Struct. Biol.* **116**, 120–130.
31. Thuman, C. P. A. and Chiu, W. (1997) Improved common line-based icosahedral particle image orientation estimation algorithms. *Ultramicroscopy* **68**, 231–255.
32. Taylor, K. A. and Glaeser, R. M. (1975) Electron diffraction of frozen, hydrated protein crystals. *Science* **186**, 1036–1037.
33. Dubochet, J., Adrian, M., Chang, J. J., Homo, J. C., Lepault, J., McDowell, A. W., and Schultz, P. (1988) Cryo-electron microscopy of vitrified specimens. *Quart. Rev. Biophys.* **21**, 129–228.
34. Jeng, T.-W., Talmon, Y., and Chiu, W. (1988) Containment system for the preparation of vitrified-hydrated virus specimen. *J. Electron Microsc.* **8**, 343–348.
35. Chiu, W. (1986) Electron microscopy of frozen, hydrated biological specimens. *Ann. Rev. Biophys. Biophys. Chem.* **15**, 237–257.
36. Downing, K. H. (1991) Spot-scan imaging in transmission electron microscopy. *Science* **251**, 53–59.
37. Brink, J., Chiu, W., and Dougherty, M. (1992) Computer-controlled spot-scan imaging of crotoxin complex crystals with 400 keV electrons at near-atomic resolution. *Ultramicroscopy* **46**, 229–240.
38. Zhou, Z. H., Prasad, B. V. V., Jakana, J., Rixon, F. J., and Chiu, W. (1994) Protein subunit structures in the herpes simplex virus A-capsid determined from 400 kV spot-scan electron cryomicroscopy. *J. Mol. Biol.* **242**, 456–469.
39. Thuman, C. P. A., Greene, B., Jakana, J., Prasad, B. V. V., King, J., Prevelige, P. E., Jr., and Chiu, W. (1996) Three-dimensional structure of scaffolding-containing phage p22 procapsids by electron cryo-microscopy. *J. Mol. Biol.* **260**, 85–98.
40. Mimori, Y., Yamashita, I., Murata, K., Fujiyoshi, Y., Yonekura, K., Toyoshima, C., and Namba, K. (1995) The structure of the R-type straight flagellar filament of Salmonella at 9 Å resolution by electron cryomicroscopy. *J. Mol. Biol.* **249**, 69–87.
41. Bottcher, B., Wynne, S. A., and Crowther, R. A. (1997) Determination of the fold of the core protein of hepatitis B virus by electron cryomicroscopy. *Nature* **386**, 88–91.
42. Conway, J. F., Cheng, N., Zlotnick, A., Wingfield, P. T., Stahl, S. J., and Steven, A. C. (1997) Visualization of a 4-helix bundle in the hepatitis B virus capsid by cryo-electron microscopy. *Nature* **386**, 91–94.

43. Frank, J., Zhu, J., Penczek, P., Li, Y., Srivastava, S., Verschoor, A., et al. (1995) Model of protein synthesis based on cryo-electron microscopy of the *E. coli* ribosome. *Nature* **376**, 441–444.
44. Zhou, Z. H., Chiu, W., Haskell, K., Spears, H., Jr., Jakana, J., Rixon, F. J., and Scott, L. R. (1998) Refinement of herpesvirus B-capsid structure on parallel supercomputers. *Biophys. J.* **74**, 576–588.
45. Baker, T. S. and Johnson, J. E. (1996) Low resolution meets high: towards a resolution continuum from cells to atoms. *Curr. Opin. Struct. Biol.* **6**, 585–594.
46. Stewart, P. L., Fuller, S. D., and Burnett, R. M. (1993) Difference imaging of adenovirus: bridging the resolution gap between X-ray crystallography and electron microscopy. *EMBO J.* **12**, 2589–2599.
47. Cheng, R. H., Reddy, V. S., Olson, N. H., Fisher, A. J., Baker, T. S., and Johnson, J. E. (1994) Functional implications of quasi-equivalence in a T = 3 icosahedral animal virus established by cryo-electron microscopy and X-ray crystallography. *Structure* **2**, 271–282.
48. Smith, T. J., Chase, E. S., Schmidt, T. J., Olson, N. H., and Baker, T. S. (1996) Neutralizing antibody to human rhinovirus 14 penetrates the receptor-binding canyon. *Nature* **383**, 350–354.
49. Cheng, R. H., Kuhn, R. J., Olson, N. H., Rossmann, M. G., Choi, H. K., Smith, T. J., and Baker, T. S. (1995) Nucleocapsid and glycoprotein organization in an enveloped virus. *Cell* **80**, 621–630.
50. Grimes, J. M., Jakana, J., Ghosh, M., Basak, A. K., Roy, P., Chiu, W., Stuart, D. I., and Prasad, B. V. (1997) An atomic model of the outer layer of the bluetongue virus core derived from X-ray crystallography and electron cryomicroscopy. *Structure* **5**, 885–893.
51. Prasad, B. V. V., Hardy, M. E., Dokland, Bella, J., M., Rossmann, M. G., and Estes, M. K. (1999) X-ray crystallographic structure of the Norwalk virus capsid. *Science*, in press.
52. Ban, N., Freeborn, B., Nissen, P., Penczek, P., Grassucci, R. A., Sweet, R., et al. (1998) A 9 Å resolution X-ray crystallographic map of the large ribosomal subunit. *Cell* **93**, 1105–1115.
53. Tao, Y., Olson, N. M., Xu, W., Anderson, D. L., Rossmann, M. G., and Baker, T. S. (1998) Assembly of tailed bacterial virus and its genome release studied in three-dimensions. *Cell* **95**, 431–437.
54. Estes, M. K., Graham, D. Y., and Mason, B. B. (1981) Proteolytic enhancement of rotavirus infectivity: molecular mechanisms. *J. Virol.* **39**, 879–888.
55. Arias, C. F., Lopez, S., and Espejo, R. T. (1982) Gene protein products of SA11 simian rotavirus genome. *J. Virol.* **41**, 42–50.
56. Zhou, Z., Crawford, S., and Estes, M. K. Personal communication.
57. Anthony, I. D., Bullivant, S., Dayal, S., Bellamy, A. R., and Berriman, J. A. (1991) Rotavirus spike structure and polypeptide composition. *J. Virol.* **65**, 4334–4340.
58. Arias, C. F., Romero, P., Alvarez, V., and Lopez, S. (1996) Trypsin activation pathway of rotavirus infectivity. *J. Virol.* **70**, 5832–5839.

59. Kaljot, K. T., Shaw, R. D., Rubin, D. H., and Greenberg, H. B. (1988) Infectious rotavirus enters cells by direct cell membrane penetration, not by endocytosis. *J. Virol.* **62**, 1136–1144.
60. Keljo, D. J., Kuhn, M., and Smith, A. (1988) Acidification of endosomes is not important for the entry of rotavirus into the cell. *J. Pediatr. Gastroenterol. Nutr.* **7**, 257–263.
61. Cohen, J. and Dobos, P. (1979) Cell free transcription and translation of rotavirus RNA. *Biochem. Biophys. Res. Commun.* **88**, 791–796.
62. Sabara, M., Ready, K. F. M., Frenchick, P. J., and Babiuk, L. A. (1987) Biochemical evidence for the oligomeric arrangement of bovine rotavirus nucleocapsid protein and its possible significance in the immunogenicity of this protein. *J. Gen. Virol.* **68**, 123–133.
63. Shen, S., Burke, B., and Desselberger, U. (1994) Rearrangement of the VP6 gene of a group A rotavirus in combination with a point mutation affecting trimer stability. *J. Virol.* **68**, 1682–1688.
64. Tosser, G., Labbé, M., Bremont, M., and Cohen, J. (1992) Expression of the major capsid protein VP6 of group C rotavirus and synthesis of chimeric single-shelled particles by using recombinant baculoviruses. *J. Virol.* **66**, 5825–5831.
65. Grimes, J., Basak, A. K., Roy, P., and Stuart, D. (1995) The crystal structure of bluetongue virus VP7. *Nature* **373**, 167–170.
66. Prasad, B. V. V. and Chiu, W. (1994) Structure of rotavirus. *Curr. Top. Microbiol. Immunol.* **185**, 9–29.
67. Labbé, M., Charpilienne, A., Crawford, S. E., Estes, M. K., and Cohen, J. (1991) Expression of rotavirus VP2 produces empty corelike particles. *J. Virol.* **65**, 2946–2952.
68. Crawford, S. E., Labbé, M., Cohen, J., Burroughs, M. H., Zhou, Y. J., and Estes, M. K. (1994) Characterization of virus-like particles produced by the expression of rotavirus capsid proteins in insect cells. *J. Virol.* **68**, 5945–5952.
69. Shaw, A. L., Samal, S. K., Subramanian, K., and Prasad, B. V. (1996) Structure of aquareovirus shows how the different geometries of the two layers of the capsid are reconciled to provide symmetrical interactions and stabilization. *Structure* **4**, 957–967.
70. Cheng, R. H., Caston, J. R., Wang, G. J., Gu, F., Smith, T. J., Baker, T. S., et al. (1994) Fungal virus capsids, cytoplasmic compartments for the replication of double-stranded RNA, formed as icosahedral shells of asymmetric Gag dimers. *J. Mol. Biol.* **244**, 255–258.
71. Valenzuela, S., Pizarro, J., Sandino, A. M., Vasquez, M., Fernandez, J., Hernandez, O., Patton, J., and Spencer, E. (1991) Photoaffinity labeling of rotavirus VP1 with 8-azido-ATP: identification of the viral RNA polymerase. *J. Virol.* **65**, 3964–3967.
72. Liu, M., Mattion, N. M., and Estes, M. K. (1992) Rotavirus VP3 expressed in insect cells possesses guanylyltransferase activity. *Virology* **188**, 77–84.
73. Chen, Z. G., Stauffacher, C., Li, Y., Schmidt, T., Bomu, W., Kamer, G., Shanks, M., Lomonosoff, G., and Johnson, J. E. (1989) Protein-RNA interactions in an icosahedral virus at 3.0 Å resolution. *Science* **245**, 154–159.
74. Tsao, J., Chapman, M. S., Agbandje, M., Keller, W., Smith, K., Wu, H., Luo, M., Rossmann, M. G., and Compans, R. W. (1991) The three-dimensional structure of canine parvovirus and its functional implications. *Science* **251**, 1456–1464.

75. McKenna, R., Xia, D., Willingmann, P., Ilag, L. L., Krishnaswamy, S., Rossmann, M. G., Olson, N. H., Baker, T. S., and Incardona, N. L. (1992) Atomic structure of single-stranded DNA bacteriophage phi X174 and its functional implications. *Nature* **355**, 137–143.
76. Fisher, A. J. and Johnson, J. E. (1993) Ordered duplex RNA controls capsid architecture in an icosahedral animal virus. *Nature* **361**, 176–179.
77. Larson, S. B., Koszelak, S., Day, J., Greenwood, A., Dodds, J. A., and McPherson, A. (1993) Double-helical RNA in satellite tobacco mosaic virus. *Nature* **361**, 179–182.
78. Labbé, M., Baudoux, P., Charpilienne, A., Poncet, D., and Cohen, J. (1994) Identification of the nucleic acid binding domain of the rotavirus VP2 protein. *J. Gen. Virol.* **75**, 3423–3430.
79. Cohen, J. (1977) Ribonucleic acid polymerase activity associated with purified calf rotavirus. *J. Gen. Virol.* **36**, 395–402.
80. Zeng, C. Q., Estes, M. K., Charpilienne, A., and Cohen, J. (1998) The N terminus of rotavirus VP2 is necessary for encapsidation of VP1 and VP3. *J. Virol.* **72**, 201–208.
81. Zeng, C. Q., Labbé, M., Cohen, J., Prasad, B. V. V., Chen, D., Ramig, R. F., and Estes, M. K. (1994) Characterization of rotavirus VP2 particles. *Virology* **201**, 55–65.
82. Bartlett, N. M., Gillies, S. C., Bullivant, S., and Bellamy, A. R. (1974) Electron microscopy study of reovirus reaction cores. *J. Virol.* **14**, 315–326.
83. Dryden, K. A., Farsetta, D. L., Wang, G., Keegan, J. M., Fields, B. N., Baker, T. S., and Nibert, M. L. (1998) Internal structures containing transcriptase-related proteins in top component particles of mammalian orthoreovirus. *Virology* **245**, 33–46.
84. Prasad, B. V. V., Yamaguchi, S., and Roy, P. (1992) Three-dimensional structure of single-shelled bluetongue virus. *J. Virol.* **66**, 2135–2142.
85. Gottlieb, P., Strassman, J., Qiao, X. Y., Frucht, A., and Mindich, L. (1990) In vitro replication, packaging, and transcription of the segmented double-stranded RNA genome of bacteriophage phi 6: studies with procapsids assembled from plasmid-encoded proteins. *J. Bacteriol.* **172**, 5774–5782.

Rotaviruses

Methods and Protocols

Gray, J.; Desselberger, U. (Eds.)

2000, X, 262 p., Hardcover

ISBN: 978-0-89603-736-6

A product of Humana Press